CHEMISTRY & CHEMICAL TECHNOLOGY

Vol. 8, No. 1, 2014 Chemistry

Oleg Figovsky[1], Dmitry Pashin[2], Zufar Khalitov[2] and Azat Khadiev[2]

THE QUANTITATIVE THEORY OF DIFFRACTION BY SPIRAL NANOTUBES

[1] Polymate Ltd., International Nanotechnology Research Center, Migdal HaEmek, Israel
[2] Kazan National Research Technical University,
10, K. Marx str., Kazan, Tatarstan 420111, Russia; pashin@addnano.ru

Received: September 03, 2012 / Revised: November 02, 2012 / Accepted: April 30, 2013

Abstract. The mathematical apparatus of simulation diffraction by spiral nanotubes of arbitrary chemical composition, whose structure is described with the use of Bravais cells, is developed. The case of electron microdiffraction by a single nanotube is considered, the distributions of intensity in layer planes and lengthways layer lines are calculated.

Keywords: spiral nanotube, layer line, chiral angle, chrysotile, electron microdiffraction.

1. Introduction

Over the last 50 years, the development of structural analysis of nanotubes by diffraction methods has been dedicated, mainly, to nanotubes of coaxial type: chiral and nonchiral nanotubes [1-3]. However, it seems obvious that the best part of synthesized nanotubes belong to spiral type: they represent cone structure or roll, when the cone angle is zero [4]. Therefore, the necessity for development of structural analysis of these abundant types of nanotubes is driven by further progress of nano-technology.

The first efforts in investigation of diffraction by spiral structures were related with two works of the middle of the last century: theoretical study performed by Jagodzinski and Kunze [5] and Whittaker's simulative optical experiments [6]. Jagodzinski and Kunze tried to solve the problem of describing spiral structure by approximation of spiral lattice by semi cylindrical layers. It is obvious that such approximation is quite rough, and diffraction from this structure will resemble diffraction from a cylindrical tube rather than from spiral.

Whittaker's simulative optical experiments made significant contributions to the investigation of spiral structures. In this experiments Whittaker performed comparison study of diffraction from artificial two-dimensional models of coaxial and spiral lattices. Due to impossibility of making real models of cylindrical lattices (because of small dimensions of the nanotube), Whittaker transferred experiment to larger dimensions – to the range of visible light. Thus, he scaled up the size of artificial models of cylindrical lattices (masks) in accordance with wave length increasing (in comparison with X-rays). Experimental results allowed him to describe and analyze azimuthal distribution peculiarity of diffraction intensities in reciprocal space of coaxial and spiral lattices and to make a conclusion that the diffraction patterns from coaxial and spiral structures are very similar and differ only in fine details [6].

The development of quantitative theory of diffraction by spiral nanotubes was being restricted for a long period of time by the lack of crystallographic description of such structures. At the beginning of this century, description within a framework of model of elastic layer was proposed, and on this basis quantitative theory of diffraction was developed [7]. However, the examination of different types of nanotubes has showed that such model is inapplicable for best parts of nanotubes, and chiral angles that correspond to the interlayer shift often have significant value.

In the recent years, the crystallographic description of spiral (roll) nanotubes within a framework of model of strong layer and with arbitrary chiral angle was made [4]. The description is based on the usage of rectangular Bravais lattice, and is applicable for nanotubes of arbitrary chemical composition. This fact is very important because of the report about synthesis of cylindrical structures that have non-hexagonal motif of atoms arrangement [8]. Bravais lattice also allows using well-known coordinates of atoms of flat analogues of nanotubes during the diffraction pattern computation.

This research is dedicated to the development of quantitative theory of diffraction by spiral nanotubes of

any chemical composition. Because of the absence of crystallographic description of cone nanotubes, the investigation is made on the basis of roll structure [4]. Detailed analysis of the problem, uncovering essential differences between diffraction from coaxial and spiral structures and comparison with experimental data will be done in our next articles.

2. Results and Discussion

2.1. The Diffraction Amplitude

Atoms of roll nanotube (Fig. 1) with arbitrary chiral angle ε_c within the model of strong layer have cylindrical coordinates [4]:

$$\begin{cases} r_{mj} = \sqrt{r_0^2 + 2t\left[\left(nb + y_j\right)\cos e_c - \left(an + z_j\right)\sin e_c\right]} + x_j \\ j_{mj} = \dfrac{1}{t}\left\{\sqrt{r_0^2 + 2t\left[\left(nb + y_j\right)\cos e_c - \left(an + z_j\right)\sin e_c\right]} - r_0\right\} \\ z_{mj} = \left(nb + y_j\right)\sin e_c + \left(an + z_j\right)\cos e_c \end{cases} \quad (1)$$

where n – index number of spiral-helical site line on the surface of the roll; v – index number of lattice site on the site line; x_j, y_j, z_j – radial, circular and longitudinal linear coordinates of j^{th} atom in Bravais cell relative to the beginning of this cell; ρ_0 – initial radius of a roll; d – thickness of the layer; $\tau = d/2\pi$; a and b – parameters (dimensions) of rectangular Bravais cell's base, where side a is chosen in the direction closest to the tube axis, and parameter b – in the direction closest to the tube cross-section (side b is perpendicular to a). Index numbers n and v are limited only by dimensions of a nanotube until the roll is not divided into the turns.

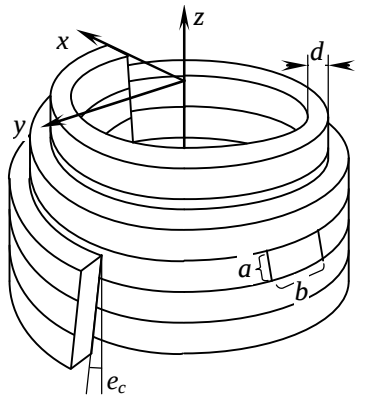

Fig. 1. Lattice parameters of roll nanotube

The diffraction amplitude in general form:

$$A\left(R, j^*, z^*\right) = \sum_{n,n,j} f_j \exp\left\{2\pi i\left[R r_{mj}\cos\left(j_{mj} - j^*\right) + z^* z_{mj}\right]\right\} \quad (2)$$

where $\{R, \varphi^*, z^*\}$ – the cylindrical coordinate system in reciprocal space of an object; $f_j(R^*)$ – the electron atomic scattering factor of j^{th} atom in Bravais cell, $R^* = \sqrt{R^2 + z^{*2}}$ – the scalar of radius-vector of a certain point in reciprocal space. From (1) and (2) it can be assumed that analytical estimation of lattice sums (over n and v) in general is complicated, and calculation of diffraction intensity that corresponds to amplitude (2) can be done only numerically.

Let us consider the structure of the nanotube in case of small chiral angle ε_c – this approach, according to [4], allows dividing spiral structure into turns. Thus, in practically important case, when generator $g = 2\pi d/b$ [4] is odd (in case of chrysotile nanotube) and $p_0 = 2\pi\rho_0/b$ is semi-integer, coordinates (1) of j^{th} atom of v^{th} primitive unit cell on m^{th} turn (index number of m begins from zero) of n^{th} spiral-helical site line in the first approximation represent a relatively simple expression:

$$\begin{cases} r_{mnj} \approx \sqrt{r_m^2 + 2t\left[nb + y_j - \left(an + z_j\right)e_c\right]} + x_j \\ j_{mnj} \approx \dfrac{1}{t}\left\{\sqrt{r_m^2 + 2t\left[nb + y_j - \left(an + z_j\right)e_c\right]} - r_m\right\} \\ z_{mnj} \approx an + \left(2\pi r_0 m + \pi d m^2 + nb + y_j\right)e_c + z_j \end{cases}$$

$$r_m = r_0 + md \quad (3)$$

where $v = 0 - (p_m\text{-}1)$; $p_m = p_0 + mg + \dfrac{g}{2}$.

Let us neglect parameter z_j in expression under radical in (3) and expand radical into a series in powers of the smallness of ε_c to the linear term and neglect parameter y_j in comparison with other terms:

$$\sqrt{r_m^2 + 2t\left[nb + y_j - \left(an + z_j\right)e_c\right]} \approx$$

$$\approx \sqrt{r_m^2 + 2t\left(nb + y_j\right)} - \frac{t\,ane_c}{\sqrt{r_m^2 + 2tnb}} \quad (4)$$

Substituting (4) into (3) and neglecting relatively small terms gives coordinates of atoms:

$$\begin{cases} r_{mnj} \approx r_{mn} + x_j = r_{mnj} \\ j_{mnj} \approx j_{mnj} - j_{mn} - j_m \\ z_{mnj} \approx an + be_c n + z_{mj} \end{cases}$$

where $r_{mn} = \sqrt{r_m^2 + 2tbn}$,

$$j_{mnj} = \frac{1}{t}\sqrt{r_m^2 + 2t\left(nb + y_j\right)},$$

$$j_{mn} = \frac{ane_c}{r_m}, \qquad j_m = \frac{r_m}{t},$$

$$z_{mj} = \left(2\pi r_0 m + \pi d m^2\right)e_c + z_j.$$

For this reason diffraction amplitude (2):

$$A(R, j^*, z^*) \approx \sum_{m=0}^{M-1} \sum_j f_j \exp(2p\, iz^* z_{mj}) \sum_{n=0}^{p_m-1} \exp(2p\, iz^* be_c n) \times$$

$$\times \sum_{n=0}^{N-1} \exp(2p\, iz^* an) \exp\left[2p\, iR r_{mnj} \cos(j_{mnj} - j^*)\right]$$

where N – the length of the nanotube in units of a and M – number of layers.

Let us expand the last exponentional function into cylindrical waves in accordance with equation

$$\exp(ia\cos g) = J_0(a) + 2\sum_{q=1}^{\infty} i^q \cos(qg) J_q(a):$$

$$A(R, j^*, z^*) = A_0(R, z^*) + A_1(R, j^*, z^*)$$

where

$$A_0(R, z^*) = \sum_{m,j} f_j \exp(2p\, iz^* z_{mj}) \times$$

$$\times \sum_n \exp(2p\, iz^* be_c n) J_0(2p\, R r_{mnj}) \sum_n \exp(2p\, iz^* an) \quad (5)$$

$$A_1(R, j^*, z^*) = 2\sum_{m,j} f_j \exp(2p\, iz^* z_{mj}) \times$$

$$\sum_n \exp(2p\, iz^* be_c n) \sum_n \exp(2p\, iz^* an) \times$$

$$\times \sum_{q=1}^{\infty} i^q \cos\left[q(j_{mnj} - j^*)\right] J_q(2p\, R r_{mnj}) \quad (6)$$

Let us consider summands of diffraction amplitude (5) and (6) sequentially. Then, let us estimate summands of q-series that make a strong contribution to amplitude of reflexes, and achieve analytic relations governing regions of existence of intensity's maxima in reciprocal space. Simulated diffraction profiles will be calculated in case of electron microdiffraction by single nanotube. We also did not take into account any fudge factors (for absorption, *etc.*) at this stage of development.

2.2. Reflexes *h*0 and *h*00

Let us consider diffraction amplitude (5). The sum taken over n has a sharp maximum when

$$z^* = \frac{h}{a}, \quad h = 0, \pm 1, \pm 2, \ldots \quad (7)$$

Such equation governs coordinates of so called «layer planes» of reciprocal space of the nanotube. Near or on this layer planes stand maxima of diffraction amplitude. When the flattish Ewald's sphere of electron beam in TEM cuts reciprocal space of the nanotube, layer planes transform into «layer lines» in diffraction pattern. Indexes of these lines coincide with the value of index h.

By using the Bessel function approximation, we can simplify our algebraic expression for finding maximum condition of sum over v:

$$J_0(x) \approx \sqrt{\frac{2}{p\, x}} \cos\left(x - \frac{p}{4}\right)$$

Therefore, with regard of expression (7):

$$\sum_n \exp\left(2p\, ih \frac{be_c}{a} n\right) J_0(2p\, R r_{mnj}) \approx$$

$$\approx \frac{1}{p\sqrt{R r_m}} \sum_n \exp\left(2p\, ih \frac{be_c}{a} n\right) \cos\left[2p\, R(r_{mn} + x_j) - \frac{p}{4}\right]$$

Let us expand ρ_{mv} into a series in powers of the smallness of its second term:

$$\sqrt{r_m^2 + 2t\, bn} \approx r_m + \frac{t\, b}{r_m} n \quad (8)$$

Therein lies the method of linear approximation for coordinates of atoms, that allows us to continue our analysis. As a result, the last sum can be cast into:

$$\sum_n \cos\left(2p\, h \frac{be_c}{a} n\right) \cos\left[2p\, R(r_{mn} + x_j) - \frac{p}{4}\right] +$$

$$+ i \sum_n \sin\left(2p\, h \frac{be_c}{a} n\right) \cos\left[2p\, R(r_{mn} + x_j) - \frac{p}{4}\right] =$$

$$= \frac{1}{2} \sum_n \left\{ \cos\left[2p\left(h \frac{be_c}{a} n + R r_{mn} + R x_j - \frac{1}{8}\right)\right] + \right.$$

$$\left. + \cos\left[2p\left(h \frac{be_c}{a} n - R r_{mn} - R x_j + \frac{1}{8}\right)\right] \right\} +$$

$$+ \frac{i}{2} \sum_n \left\{ \sin\left[2p\left(h \frac{be_c}{a} n + R r_{mn} + R x_j - \frac{1}{8}\right)\right] + \right.$$

$$\left. + \sin\left[2p\left(h \frac{be_c}{a} n - R r_{mn} - R x_j + \frac{1}{8}\right)\right] \right\}$$

These sums have maxima when

$$p\, b\left(\frac{h}{a} e_c \pm R \frac{t}{r_m}\right) = kp \quad \Rightarrow$$

$$\Rightarrow R = \pm \frac{1}{d}\left(k \frac{2p\, r_m}{b} - \frac{h}{a} 2p\, r_m e_c\right), \quad k = 0, \pm 1, \pm 2, \ldots$$

The first term in brackets is approximately equal to kp_m having relative high value that, even after dividing by d, goes far beyond the scope of limits of considered region of R coordinate. Therefore, $k = 0$ and the amplitude (5) governs strong reflexes [9, 10]. The next term corresponds to locations of maxima of m^{th} summands of the diffraction amplitude of h00 reflex for monoclinic, and when $\varepsilon_c = 0$ – for an orthogonal polytypic modification of nanotube structure [4].

Consequently, the amplitude (5) governs series of pseudoorthogonal h0 [9] and h00 reflexes from a roll nanotube in case of strong layer. Arithmetical sign « ± » provides positive value of R coordinate in both sides of reciprocal space of an object, where layer planes with $h < 0$ and $h > 0$ stand. In the case of $h > 0$ we must choose negative value. With these results we can estimate expression for amplitude (5):

$$A_S^{h00}(R) = N\sum_j f_j \sum_{m=0}^{M-1} \exp\left(2p\,i\frac{h}{a}z_{mj}\right)\times$$
$$\times\sum_{v=0}^{p_m-1}\exp\left(2p\,i\frac{h}{a}be_c n\right)J_0\left(2p\,R\,r_{mnj}\right)$$

where N – value of sum over n, index S signify that these reflexes are strong.

Fig. 2 shows calculated profiles of the beginning of 2nd layer line for monoclinic roll nanotubes with different chiral angles. Each curve is a summation of pseudoorthogonal $h0$ and monoclinic $h00$ reflexes (when the chiral angle is small reflexes merge with each other). The pseudoorthogonality effect was analyzed earlier in case of chiral and nonchiral nanotubes [9, 10]. In this case, as for nonchiral nanotubes, pseudoorthogonal reflexes are formed by primary maximum of Bessel functions with zero index and thus reflexes are located in $R = 0$.

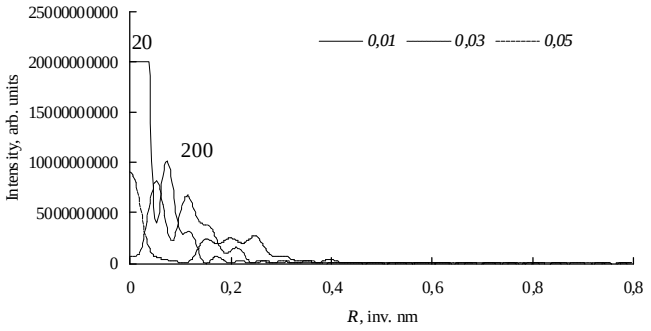

Fig. 2. Profiles of the beginning of 2nd layer line of monoclinic roll nanotubes with different chiral angles ε_c (degrees). The maximum intensity ($1.69\cdot10^{11}$) is synthetically limited

Let us consider the amplitude (6) and related diffraction effects.

2.3. Reflexes of General Position

The amplitude (6) can be cast into such form:

$$A_1\left(R, j^*, z^*\right) = \sum_{m,j} f_j \exp\left(2p\,iz^* z_{mj}\right)\sum_q i^q\times$$
$$\times\sum_n \exp\left(2p\,iz^* be_c n\right)J_q\left(2p\,R\,r_{mnj}\right)\times$$
$$\times\left\{\exp\left[iq\left(j_{mnj} - j_m - j^*\right)\right]\sum_n \exp\left[2p\,i\left(z^* - \frac{qe_c}{2pr_m}\right)an\right] +\right.$$
$$\left.+\exp\left[-iq\left(j_{mnj} - j_m - j^*\right)\right]\sum_n \exp\left[2p\,i\left(z^* + \frac{qe_c}{2pr_m}\right)an\right]\right\} \quad (9)$$

Sums over n have sharp maxima when

$$p\,a\left(z^* \pm \frac{qe_c}{2pr_m}\right) = hp \;\Rightarrow$$
$$\Rightarrow z_m^* = \frac{h}{a}\mathbf{m}\frac{qe_c}{2pr_m},\; h = 0, \pm1, \pm2, \ldots \quad (10)$$

By introducing the following notation

$$S_{mq}^{\pm} = \sum_{n=0}^{N-1}\exp\left[2p\,i\left(z^* \pm \frac{qe_c}{2pr_m}\right)an\right] \quad (11)$$

we reduce the amplitude (9) to

$$A_1\left(R, j^*, z^*\right) = \sum_{m,j} f_j \exp\left(2p\,iz^* z_{mj}\right)\sum_q i^q\times$$
$$\times\left\{\exp\left[-iq\left(j_m + j^*\right)\right]S_{mq}^-\times\right.$$
$$\times\sum_n \exp\left(2p\,iz^* be_c n + iqj_{mnj}\right)J_q\left(2p\,R\,r_{mnj}\right) +$$
$$+\exp\left[iq\left(j_m + j^*\right)\right]S_{mq}^+\sum_n \exp\left(2p\,iz^* be_c n -\right.$$
$$\left.\left.-iqj_{mnj}\right)J_q\left(2p\,R\,r_{mnj}\right)\right\} \quad (12)$$

For estimation of the maximum condition of lattice sums over v, we should use the Bessel function approximation:

$$J_q(x) \approx \begin{cases}\cos\left(x - \frac{p}{2}q\right), & x \geq q\\ 0, & x < q\end{cases}$$

It allows us to reduce sums over v in expression (12) to:

$$S_{mqj}^{\pm} \approx \frac{1}{2}\sum_{n=0}^{p_m-1}\exp\left[i\left(2p\,z^* be_c n \pm\right.\right.$$
$$\left.\left.\pm qj_{mnj}\right)\right]\left\{\exp\left[i\left(2p\,R\,r_{mnj} - \frac{p\,q}{2}\right)\right] +\right.$$
$$\left.+\exp\left[-i\left(2p\,R\,r_{mnj} - \frac{p\,q}{2}\right)\right]\right\} \quad (13)$$

For further analysis we use linear approximation again. Let us expand φ_{mvj} into a series in powers of the smallness of $2\tau(bv + y_j)$ to the linear term:

$$\sqrt{r_m^2 + 2t\left(bn + y_j\right)} \approx r_m + \frac{t\,b}{r_m}n + \frac{t\,y_j}{r_m}$$

and use also the expansion (8). Thus, when $2\pi R\rho_m \geq q$, sums (13) may be expressed as following:

$$S_{mqj}^{\pm} \approx A_{mqj}^{\pm}B_{mqj}^{+}\sum_{n=0}^{p_m-1}\exp\left[i\left(2p\,z^* be_c + 2p\,R\frac{t\,b}{r_m} \pm \frac{qb}{r_m}\right)n\right] +$$
$$+A_{mqj}^{\pm}B_{mqj}^{-}\sum_{n=0}^{p_m-1}\exp\left[i\left(2p\,z^* be_c - 2p\,R\frac{t\,b}{r_m} \pm \frac{qb}{r_m}\right)n\right] \quad (14)$$

Where $A_{mqj}^{\pm} = \frac{1}{2}\exp\left[\pm iq\left(j_m + \frac{y_j}{r_m}\right)\right]$,

$$B_{mqj}^{\pm} = \exp\left[\pm i\left(2p\,R r_m + 2p\,R x_j - \frac{p\,q}{2}\right)\right]$$

The upper arithmetical sign in arguments of exponential functions and in value $A_{mqj}^{\pm}$ corresponds to the first term of amplitude (12), and lower – to the second term.

Consequently, the amplitude (12) can be cast into such form:

$$A_1\left(R, j^*, z^*\right) \approx \sum_{m,j} F_{mj} \sum_q i^q \left\{\exp\left[-iq\left(j_m + j^*\right)\right] S_{mq}^- S_{mqj}^+ + \exp\left[iq\left(j_m + j^*\right)\right] S_{mq}^+ S_{mqj}^- \right\} =$$

$$= \sum_{m,j} F_{mj} \sum_q i^q \left\{\exp\left[-iq\left(j_m + j^*\right)\right] S_{mq}^- A_{mqj}^+ B_{mqj}^+ \times \right.$$

$$\times \sum_{n=0}^{p_m - 1} \exp\left[i\left(2p\,z^* b e_c + 2p\,R\frac{t\,b}{r_m} + \frac{qb}{r_m}\right)n\right] +$$

$$+ \exp\left[-iq\left(j_m + j^*\right)\right] S_{mq}^- A_{mqj}^+ B_{mqj}^- \times$$

$$\times \sum_{n=0}^{p_m - 1} \exp\left[i\left(2p\,z^* b e_c - 2p\,R\frac{t\,b}{r_m} + \frac{qb}{r_m}\right)n\right] +$$

$$+ \exp\left[iq\left(j_m + j^*\right)\right] S_{mq}^+ A_{mqj}^- B_{mqj}^+ \times$$

$$\times \sum_{n=0}^{p_m - 1} \exp\left[i\left(2p\,z^* b e_c + 2p\,R\frac{t\,b}{r_m} - \frac{qb}{r_m}\right)n\right] +$$

$$+ \exp\left[iq\left(j_m + j^*\right)\right] S_{mq}^+ A_{mqj}^- B_{mqj}^- \times$$

$$\left. \times \sum_{n=0}^{p_m - 1} \exp\left[i\left(2p\,z^* b e_c - 2p\,R\frac{t\,b}{r_m} - \frac{qb}{r_m}\right)n\right]\right\} \quad (15)$$

where $F_{mj} = f_j \exp\left(2p\,i z^* z_{mj}\right)$.

Sums over v in the expression (15) have sharp maxima when

$$z^* e_c \pm R\frac{t}{r_m} \pm \frac{q}{2p r_m} = \frac{k}{b},\ k = 0, \pm 1, \pm 2, \ldots \quad (16)$$

Therefore, the diffraction amplitude consist of four summands, each of which contains product of sum over n ($S_{mq}^{\pm}$ multiplier) by sum over v. Maxima of amplitude could be achieved when conditions (10) and (16) are fulfilled simultaneously. These conditions generate a set of equations for defining z^* and q. Results of defining q for four summand of the amplitude (15) are noted in fourth column in the Table, in which we neglected a value containing e_c^2 multiplier.

By substituting q from the fourth column into the second, and by neglecting summands of second order of smallness (values of first order of smallness are ε_c and $1/2\pi\rho_m$), we can achieve coordinates of layer lines

$$z^* \approx \frac{h}{a} + \frac{k}{b} e_c \quad (17)$$

for all four terms, where it is necessary to take into account arithmetical signs of k and ε_c. From (17) we see that in this case, in comparison with diffraction by chiral nanotubes, coordinates of layer lines in a first approximation are independent of the layer number m.

Let us consider the fourth column of the Table. It is obvious that among the three summands contributing to q, the first summand has the largest on modulus value, when $k \neq 0$. Thus, this summand governs arithmetical sign of q. By taking into account the fact that $q \geq 1$ by convention, it may be deduced that 1st and 2nd summands of amplitude (15) govern reflexes with $k > 0$, and 3th and 4th - with $k < 0$. In consequence of $R \geq 0$ by convention, the amplitude of strong reflexes is governed by 2nd and 3th summands when $k = 0$. Because of symmetry of reciprocal space, we will consider only layer lines with $h \geq 0$.

Table

Values of z^* and q, at which maxima of amplitude are reached

Summand number	Maximum condition for sum over n	Maximum condition for sum over v	q
1	$z_m^* = \frac{h}{a} + \frac{q e_c}{2p r_m}$	$z^* e_c + R\frac{t}{r_m} + \frac{q}{2p r_m} = \frac{k}{b}$	$q_1 = k\frac{2p r_m}{b} - 2p r_m \frac{h}{a} e_c - Rd$
2		$z^* e_c - R\frac{t}{r_m} + \frac{q}{2p r_m} = \frac{k}{b}$	$q_2 = k\frac{2p r_m}{b} - 2p r_m \frac{h}{a} e_c + Rd$
3	$z_m^* = \frac{h}{a} - \frac{q e_c}{2p r_m}$	$z^* e_c + R\frac{t}{r_m} - \frac{q}{2p r_m} = \frac{k}{b}$	$q_3 = -k\frac{2p r_m}{b} + 2p r_m \frac{h}{a} e_c + Rd$
4		$z^* e_c - R\frac{t}{r_m} - \frac{q}{2p r_m} = \frac{k}{b}$	$q_4 = -k\frac{2p r_m}{b} + 2p r_m \frac{h}{a} e_c - Rd$

Therefore, our estimation shows that strong reflexes of the diffraction pattern from a roll nanotube with small chiral angle stand on layer lines (7), and diffuse reflexes are shifted from lines by the value proportional to chiral angle in direction corresponding to its sign and sign of *k* index. By considering the fourth column as a rule for choosing terms of series over *q* in the amplitude (12), we will get expressions for the amplitude of strong reflexes.

2.4. Strong Reflexes of Zero Layer Line

From the Table for $h = k = 0$ we can estimate *q*: $q_2 = q_3 = Rd$, and, keeping in mind that *q* must be integer, we can get an expression:

$$q_2 = q_3 = l \quad \Rightarrow R_l = \frac{l}{d}, \qquad l = 1, 2, 3, \ldots \tag{18}$$

This expression describes locations of so called «basal» reflexes 00*l* on the layer line with $z^* = 0$. Therefore, 00*l* reflexes are described by primary summands of series over *q* in the expression (12), moreover each reflex is described by its own summand with $q = l$. As a result, in case of inessential overlap of Bessel functions the amplitude (12) can be written as:

$$A_S^{00l}\left(R, j^*\right) = 2i^l N \sum_{m,j} f_j \sum_n \cos\left[l\left(j_{mnj} - j_m - j^*\right)\right] J_l\left(2\pi R r_{mnj}\right)$$

where maxima of $S_{ml}^{\pm}$ equal to *N* are taken into account. Corresponding intensity

$$I_S^{00l}\left(R, j^*\right) = 4N^2 \left\{\sum_j f_j \sum_{m=0}^{M-1} \sum_{v=0}^{p_m-1} \cos\left[l\left(j_{mnj} - j_m - j^*\right)\right] J_l\left(2\pi R r_{mnj}\right)\right\}^2 \tag{19}$$

is independent of chiral angle, but has an angular dependence to φ^*. Fig. 3 shows profiles of 00*l* reflexes calculated from the expression (19). It is interesting to note that only 00*l* reflex has small-angle tail.

2.5. Strong Reflexes Standing on the Layer Lines with $h > 0$

Here from the Table and for $k = 0$ we can estimate:

$$q_2 = Rd - 2\pi r_m \frac{h}{a} e_c, \; q_3 = Rd + 2\pi r_m \frac{h}{a} e_c \tag{20}$$

Integrality requirement for *q* gives:

$$R_{h0l} = \frac{l}{d} \pm h \frac{2\pi r_m e_c}{ad}$$

where *l* is governed by the expression (18).

Thus in this case, as in the preceding subject, strong reflexes *h*0*l* (except *h*00 reflexes) are also described by primary terms of series over *q* in the expression (12). However, by comparing with similar expressions for monoclinic polytypic modifications of circle, chiral and also spiral nanotubes in model of elastic layer, it is easy to see that the variable $2\pi\rho_m\varepsilon_c$ plays the role of interlayer shift Δz. Taking into account the result of the Section 2.2. of the article, we can write an expression for locations of maxima of m^{th} summands of strong reflexes *h*0*l* on the layer line in traditional way [9]:

$$R_{h0l} = \frac{1}{d}\left|l + h\frac{2\pi r_m e_c}{a}\right|, \; l = 0, \pm1, \pm2, \ldots$$

In the same way as in the previous section of sum (11) let us set:

$$S_{mq_2}^{\pm} \approx S_{mq_3}^{\pm} \approx N$$

and the amplitude (12) for $q = l$, $l = 1, 2, \ldots$, can be conceived of as:

$$A_S^{h0l}\left(R, j^*\right) \approx 2Ni^l \sum_{m,j} f_j \exp\left(2\pi i h \frac{z_{mj}}{a}\right) \times$$
$$\times \sum_n \exp\left(2\pi i h \frac{be_c}{a} n\right) \cos\left[l\left(j_{mnj} - j_m - j^*\right)\right] \times$$
$$\times \left|\cos\left[l\left(j_{mnj} - j_m - j^*\right)\right]\right| J_l\left(2\pi R r_{mnj}\right) \tag{21}$$

This expression for $h = 0$ is totally identical to (19). Thus, expression (21) governs amplitudes of couples of strong reflections $h0l - h0\bar{l}$ from roll monoclinic nanotube with small chiral angle in the model of strong layer.

Fig. 4 shows profiles of reflexes 20+200 taken from Fig. 2, and profiles of 20*l* reflexes calculated for intensity corresponding to the amplitude (21), with structural parameters of chrysotile and different chiral angles. As expected during the analysis, the diffraction profile is a summation of pair $h0\bar{l} - h0l$ reflexes for $l > 0$ and $\varepsilon_c = -0.04^{\circ}$. In case of the orthogonal polytypic modification of roll nanotube ($\varepsilon_c = 0$), reflexes from pairs join together and make a summary single reflex, which is routinely [11] identified as *h*0*l* reflex.

Increasing of chiral angle leads to degradation of diffraction conditions (Fig. 4). It must be emphasized that such effect is not a result of our approximations. It is obvious that within the framework of the assumed model small angle ε_c is a good simulation parameter. However, from (3) it follows that increasing of chiral angle will lead to strong change in z coordinates of atoms from one layer to another. This leads to "destruction" of scattering planes *h*0*l* and, as a result, to deterioration of diffraction conditions.

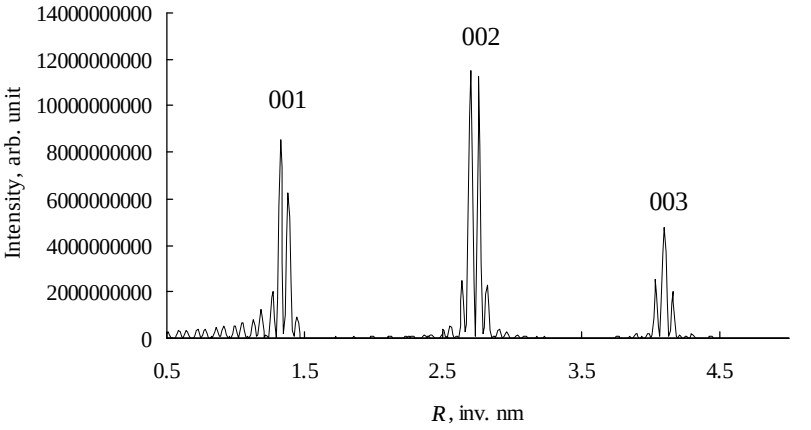

Fig. 3. Strong reflexes of zero layer line from roll nanotube for $\varphi^* = 0$

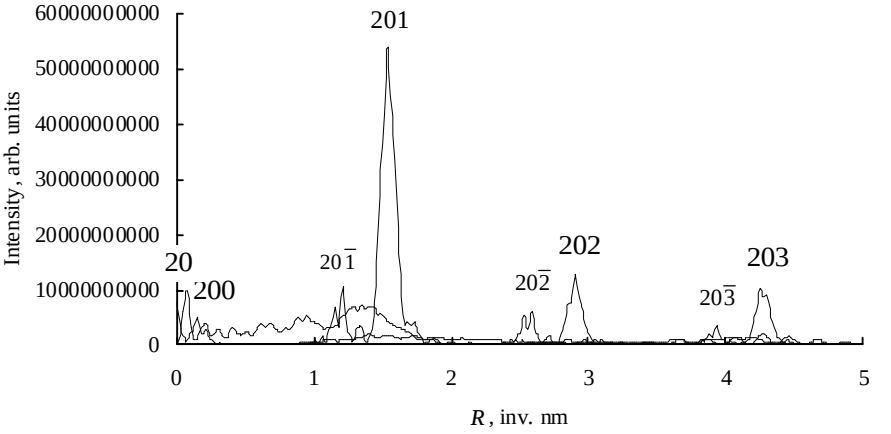

Fig. 4. Strong reflexes on the second layer line from chrysotile monoclinic roll nanotube with $\varphi^* = 0$ and $\varepsilon_c = -0.04^o$ (solid line), -0.5^o (dotted line) and -1^o (dashed line)

2.6. Diffuse Reflexes

Locations of layer lines of diffuse reflexes are governed by the expression (17) with regard to algebraic sign of k index. The amplitude (12) describes the profile of diffuse reflex $hk0$. In this amplitude selection of terms of series over q should be done in accordance with the Table: q_1 and q_2 – for $k > 0$, and q_3, q_4 – for $k < 0$. However, selection of terms of series that contribute significantly to diffraction amplitude must be done in slightly complicated way – this way will be discussed below.

Our findings allow estimating locations of main maxima of diffuse reflexes. Let us use one of the well known properties of the Bessel function, which lies in the fact that its main maximum located near the value of an argument equal to index of the function. For the amplitude (12) and noted in the Table q this gives:

$$\begin{aligned} k > 0: \quad & R_{hk0} \approx \frac{k}{b} - \frac{h}{a} e_c \\ k < 0: \quad & R_{h\bar{k}0} \approx \frac{-k}{b} + \frac{h}{a} e_c \end{aligned} \tag{22}$$

where we neglect relatively small values. By comparing expressions (17) and (22) it is easy to see that for $\varepsilon_c > 0$ reflex $hk0$ lies above the layer line with $z^* = h/a$ and at smaller values of R, and $h\bar{k}0$ reflex – under the layer line with biggest R. For $\varepsilon_c < 0$ reflexes will interchange places.

For estimation of an angular splitting relatively to the centre of reciprocal space of such reflexes in microdiffraction pattern, we determine the formula for scalar vector of main maximum of diffuse reflex from (17) and (22):

$$R^*_{hk0} = \sqrt{R^2_{hk0} + z^{*2}} \approx \sqrt{\left(\frac{k}{b}\right)^2 + \left(\frac{h}{a}\right)^2} \tag{23}$$

The splitting is independent on the value of the chiral angle. It means that the splitting of diffuse reflexes occurs on the arc of a circle with the center coinciding with the centre of reciprocal space. From (17) and (22) it also follows that the distance between two main maxima of diffuse reflexes having opposite signs of k index may be written as:

$$\Delta^* = 2e_c\sqrt{\left(\frac{k}{b}\right)^2+\left(\frac{h}{a}\right)^2} \qquad (24)$$

Sought value of splitting angle can be estimated from (23) and (24):

$$\frac{\Delta^*}{R^*_{hk0}} \approx 2e_c$$

Let us get quantitative expressions describing diffuse reflexes. The integrality requirement of q and results of previous sections give that each m^{th} summand of amplitude of diffuse reflex is described by the group of terms of the series over q in the amplitude (12). Each group consists of terms, q-indexes of which are varied sequentially near the value $|k|(p_0+mg)$. Limits of this group can be easily obtained from the last column in the Table:

$$q \approx \left[|k|(p_0+mg)-l_{\max}\right] \div |k|(p_0+mg)+l_{\max}\Big] \qquad (25)$$

where $l_{\max}$ – the smallest integer greater than Rd, that is used during simulation.

Indexes of corresponding Bessel functions in the amplitude (12) also differ by one, and for this reason, these functions are closely adjacent to each other in R scale. This means that we can not neglect their overlap, and therefore, we must add diffraction amplitudes rather than diffraction intensities. On the other hand, for increment of k difference between indexes of two adjacent groups correspond to the value $|k|(p_0+mg)$. In case of such significant distance in R scale and inessential overlap of Bessel functions, we may consider diffraction amplitudes of diffuse reflexes independently of each other.

Note that in this case q indexes of terms of the series that governs diffuse reflexes are not small, therefore we can not neglect second term in round brackets of sums (11), as we did in case of strong reflexes. For this reason maximum condition of sums gives:

$$p\left(z^* \pm \frac{qe_c}{2pr_m}\right)a = hp \;\Rightarrow\; z^* = \frac{h}{a}\mathbf{m}\frac{q}{2pr_m}e_c \approx \frac{h}{a}\mathbf{m}\frac{k}{b}e_c$$

where k should be taken modulo.

By comparing this expression with (17), it may be concluded that in case of diffuse reflexes, S^-_{mq} sum corresponds to reflexes with $k > 0$ and S^+_{mq} - to reflexes with $k < 0$.

Taking into account the expression (17), the amplitude (12) in case of diffuse reflex with $k > 0$, it can be conceived of as:

$$A_D^{hk0}(R,j^*) \approx N\sum_{q,m,v,j} f_j\left[i^q\cos g_{qmvj}J_q\left(2pRr_{mnj}\right)+ + i^{q+1}\sin g_{qmvj}J_q\left(2pRr_{mnj}\right)\right] \qquad (26)$$

where D index means "diffuse" and

$$g_{qmvj} = 2p\left(\frac{h}{a}+\frac{q}{2pr_m}e_c\right)\left(z_{mj}+be_cn\right)+q\left(j_{mnj}-j_m-j^*\right).$$

A similar estimation can be made for diffuse reflex with $k < 0$:

$$A_D^{h\bar{k}0}(R,j^*) \approx N\sum_{q,m,v,j} f_j\left[i^q\cos g_{qmvj}J_q\left(2pRr_{mnj}\right)+ + i^{q+1}\sin g_{qmvj}J_q\left(2pRr_{mnj}\right) \qquad (27)$$

where

$$g_{qmvj} = 2p\left(\frac{h}{a}-\frac{q}{2pr_m}e_c\right)\left(z_{mj}+be_cn\right)-q\left(j_{mnj}-j_m-j^*\right).$$

Limits of summation over q in expressions (26) and (27) are defined by the expression (25).

Let us consider peculiarities of the intensity distribution of diffuse reflexes in cross-section (relatively to the axis of nanotube) of reciprocal space of a roll nanotube. For theoretical estimation the Bessel function has to be approximated by cosine. Terms and multipliers that contribute a significant value to estimation of the amplitude (27) for $q \approx kp_m$ are then approximately represented by

$$\sum_m i^{kp_m}\cos\left(2p\frac{h}{a}2pr_0me_c - kp_mj^* \pm 2pRr_m\right)$$

Addition of summands in real and imaginary parts of the amplitude depends on the parameter kgm. It is obvious that for even kg cosinusoidal summands come only into real part of the amplitude and sinusoidal – only into imaginary part. In case of odd kg summands come into real and imaginary part alternately. In that case we should change m to $2m$ and modify the limits of summation. In this analysis limit of summation does not matter, and therefore, considering the expression can be approximated by

$$\sum_m \cos\left[2\left(\frac{2ph}{a}2pr_0e_c - kgj^* \pm 2pRd\right)m + A\right]$$

where A contains summands that are independent of summation index.

Sums have maxima when

$$\frac{2ph}{a}2pr_0e_c - kgj^* \pm 2pRd = np$$

where n – integer.

This expression is equation for the class of right-handed and left-handed Archimedean spirals are arranged in layer plane (17) in reciprocal space. Let us deduce φ^* from the expression near the spiral beginning, where $R \approx |k|/b$ (since we wish to study points where spirals begin we should consider only right-handed spirals):

$$j^* = -\frac{p}{kg}n + \frac{2p\,h}{a}\cdot\frac{2pr_0}{kg}e_c + \frac{2p\,d}{kg}R \approx$$

$$\approx -\frac{p}{kg}n + \frac{2p\,h}{a}\cdot\frac{2pr_0}{kg}e_c + \frac{|k|}{k}$$

From the first term at the right side of the equation it follows that the pattern is repeated every π/kg angle and it turns out that it has $2kg$-fold symmetry. It is easy to see that for even kg in imaginary and real parts of amplitude summands are twice as much and this yields that the pattern has a kg-fold symmetry. Therefore, the pattern has a symmetry center in both cases. Note that we can use such analytic simplification only for qualitative evaluation, but not for exact calculation.

Obtained results allow us to pass to simulation of diffraction profiles of diffuse reflexes along the layer line using (26) and (27). For this purpose according to (17) it is necessary to choose z^* coordinate of layer line and azimuthal angle φ^*, at which the reciprocal space of the nanotube is cut by Ewald's sphere of electron beam.

Fig. 5 shows simulated distribution of intensity of 110 diffuse reflex from the roll orthogonal chrysotile nanotube in the $\{R, \varphi^*\}$ plane with coordinate z^* expressed in (17). In accordance with our estimation this distribution has a helical fashion that is very similar to diffuse reflexes from coaxial nanotubes [9, 10]. Distortion of $2kg$-fold symmetry (generator g of chrysotile is equal to 5) on the lower levels of intensity connected with existence of the end points of spiral lattice in $\{\rho, \varphi\}$ plane, angle locations of which in this simulation are agreed.

Fig. 6 shows simulated profiles of 110 reflex along the layer line (17) for different φ^*, showed in Fig. 5 by straight lines of the same type. From the picture it follows that the profile of diffuse reflex depends on the nanotube orientation relatively to electron beam. This peculiarity has a significant importance for lattice parameters (b) measuring technique that uses microdiffraction pattern from single nanotube.

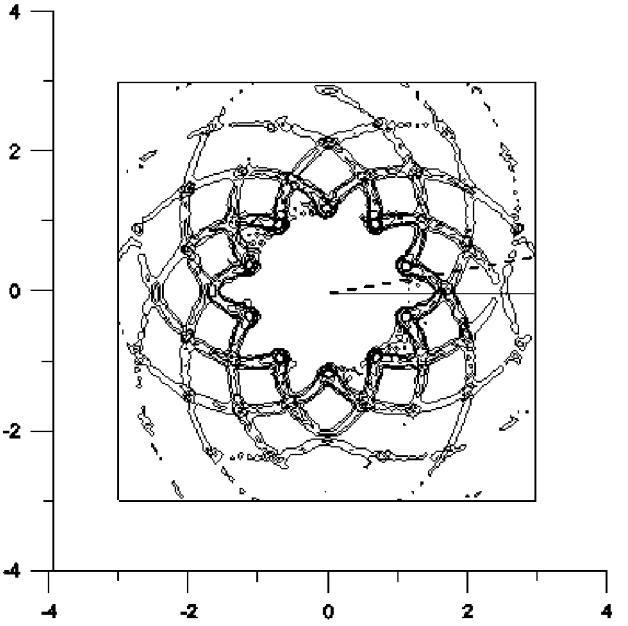

Fig. 5. Simulated distribution of intensity of 110 diffuse reflex from roll chrysotile nanotube in the $\{R, \varphi^*\}$ plane

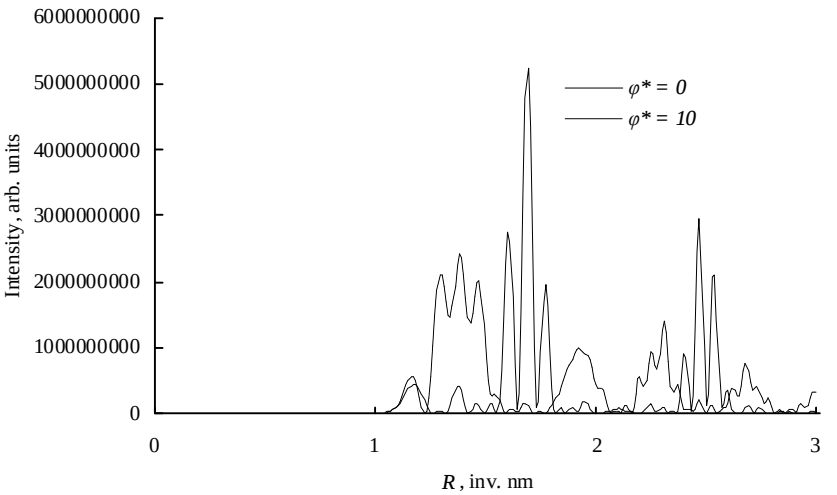

Fig. 6. Simulated profiles of 110 diffuse reflex for different φ^* showed in Fig. 5 by straight lines of the same type

The truth is that any of several points of the beginning of pair spiral reflexes in Fig. 5 could be associated with the main maximum of diffuse reflex *hk*0. Its polar radius is about $R_{hk0} \approx k/b$, and here "≈" sign means that the point is slightly shifted from the k/b value in the direction of large R according to average radius of the nanotube [12]. However, for random orientation of the nanotube relatively to its axis, every point of intersection between spiral-reflex and Ewald's sphere could be the maximum of diffuse reflex in the microdiffraction pattern. This may cause serious errors while measuring lattice parameters.

The presented diffraction theory also allows explaining the origin of local maxima of intensity in the region of "tails" of diffuse reflexes that typically occurs in microdiffraction patterns from single nanotube. The performed analysis and simulated profiles in Figs. 5 and 6 demonstrate that it is a result of cutting of spiral reflexes set, that represents diffuse reflex, by Ewald's sphere. The maxima indexing problem and the peculiarities of spiral reflexes will be considered in the next articles of this series.

3. Conclusions

The examination of purposed theory of diffraction by spiral (scroll) nanotubes in case of small chiral angle was done. Peculiarities of diffraction by spiral (scroll) nanotubes resemble diffraction from coaxial nanotubes with some exceptions. In case of spiral nanotubes strong reflections of zero layer line have angular dependence whereas diffraction by coaxial nanotubes doesn't have such peculiarity. Further investigations of differences in diffraction from spiral and coaxial nanotubes will be done in the next articles of this series.

References

[1] Deniz H., Derbakova A. and Qin L.-C.: Ultramicroscopy, 2010, **111**, 66.
[2] Deniz H. and Qin L.-C.: Chem. Phys. Lett., 2012, **552**, 92.
[3] Qin L.-C.: Reports Prog. Phys., 2006, **69**, 2761.
[4] Nasyrov I., Pashin D., Khalitov Z. and Valeeva D.: Sci. Israel-Techn. Adv., 2010, **12**, 63.
[5] Jagodzinski H. and Kunze G.: News Jb. Mineral. Mh., 1954, 95.
[6] Whittaker E.: Acta Cryst., 1955, **8**, 265.
[7] Galimov E. and Khalitov Z.: Modelirovanie Difrakcii Nanotrubkami. Izd-vo Kazan. Gos. Techn. Univ., Kazan 2007.
[8] Radovsky G., Popovitz-Biro R., Staiger M. *et al.*: Angew. Chem. Intl. Edn., 2011, **50**, 12316.
[9] Figovsky O., Pashin D., Nasyrov I. *et al.*: Chem. & Chem. Techn., 2012, **6**, 43.
[10] Figovsky O., Pashin D., Khalitov Z. *et al.*: Chem. & Chem. Techn., 2012, **6**, 167.
[11] Gricaenko G., Zviagin B., Boiarskaia R. *et al.*: Metody Elektronnoi Microskopii Mineralov. Nauka, Moskwa 1969.
[12] Wittaker E.: Acta Cryst., 1967, **10**, 149.

КІЛЬКІСНА ТЕОРІЯ ДИФРАКЦІЇ НА СПІРАЛЬНИХ НАНОТРУБКАХ

Анотація. *Розроблено математичну модель дифракції на спіральних нанотрубках довільного хімічного складу, структура яких описується з використанням комірок Браве. Розглянуто випадок мікродифракції електронів на окремій нанотрубці, розрахований розподіл інтенсивності в площині шарів і вздовж ліній шарів.*

Ключові слова*: спіральна нанотрубка, лінія шару, хіральний кут, хризотил, мікродифракція електронів.*